Available online at www.sciencedirect.com
SCIENCE DIRECT
Polyhedron 25 (2006) 2207–2214
POLYHEDRON
www.elsevier.com/locate/poly

Thallium complexes of tetraphenylporphyrin: Tl(tpp-*N*-O)(OAc) and *cis*-acetato-N-*p*-*tert*-butylbenzensulfonylimido-*meso*-tetraphenylporphyrinatothallium(III) Tl(N-*p*-$NSO_2C_6H_4{}^tBu$-tpp)(OAc)

Fuh-An Yang [a], Kuan-Yu Cho [a], Jyh-Horung Chen [a,*], Shin-Shin Wang [b,*], Jo-Yu Tung [c], Hsi-Ying Hsieh [c], Feng-Ling Liao [d], Gene-Hsiang Lee [e], Lian-Pin Hwang [f], Shanmugam Elango [g]

[a] *Department of Chemistry, National Chung-Hsing University, Taichung 40227, Taiwan*
[b] *Union Chemical Laboratories, Hsin-Chu 300, Taiwan*
[c] *Chung Hwa College of Medical Technology, Tainan 717, Taiwan*
[d] *Department of Chemistry, National Tsing-Hua University, Hsin-Chu 300, Taiwan*
[e] *Instrumentation Center, National Taiwan University, Taiwan*
[f] *Department of Chemistry, National Taiwan University and Institute of Atomic and Molecular Sciences, Academia Sinica, Taipei 10764, Taiwan*
[g] *Institute of Chemical and Engineering Sciences, Singapore 627833, Singapore*

Received 9 December 2005; accepted 10 January 2006
Available online 7 March 2006

Abstract

The crystal structures of Tl(tpp-*N*-O)(OAc) (**3**) and acetato-N-*p*-*tert*-butylbenzensulfonylimido-*meso*-tetraphenylporphyrinatothallium(III) Tl(N-*p*-$NSO_2C_6H_4{}^tBu$-tpp)(OAc) (**5**) have been determined. The coordination sphere around Tl^{3+} is a distorted square-based pyramid in which the apical site is occupied by a bidentate chelating OAc^- group for **3** and **5**. The plane of three pyrrole nitrogen atoms (i.e., N(1), N(2) and N(3)), strongly bonded to Tl^{3+} in **3** and **5**, is adopted as a reference plane, 3*N*. The porphyrin ring is severely distorted and the pyrrole ring N(4) bonding to the oxygen and $NSO_2C_6H_4{}^tBu$ group makes a dihedral angle of 46.5° and 46.7° with the 3*N* plane for **3** and **5**, respectively. In **3**, Tl^{3+} and O(1) are located on the same side at 1.11 and 1.34 Å from its 3*N* plane, and in **5**, Tl^{3+} and N(5) are also located on the same side at 1.15 and 1.30 Å from its 3*N* plane. The free energy of activation at the coalescence T_c for the intermolecular acetate exchange process of **3** and **5** in CD_2Cl_2 is found to be $\Delta G^{\ddagger}_{184} = 39.3$ and $\Delta G^{\ddagger}_{208} = 44.1$ kJ/mol, respectively, through ^1H NMR variable temperature measurements.

An electronegative substituent, O(1), bonded to Tl in **3** causes a significant negative contribution up to 145 Hz for Δ^3J(Tl–C, O) and 79 Hz for Δ^2J(Tl–C, O) for OAc^- in **3**.

Keywords: Thallium; X-ray diffraction; N-oxide; Torsion angle; Dynamic NMR

1. Introduction

Metalloporphyrins with a bridged structure between the central metal and one of the four pyrrole nitrogens have drawn much attention in recent times and so far bridged metalloporphyrins with a metal–O–N linkage (metal = Ni [1]), metal–N–N linkage (metal = Zn [2–4], Ni [5,6], Fe [3,7], Tl [5,8,9], Ga [8,9]) and metal–C–N linkage (metal = Fe [10]) have been reported. Balch and coworkers reported that the insertion of nickel(II) into H_2(OEP-*N*-O) (OEP = dianion of octaethylporphyrin) produced the complex Ni(OEP-*N*-O) (**1**), in which the metal ions are bound to a nearly planar set of three nitrogen atoms and one oxygen atom [1,11]. Upon replacing OEP^{2-} with tpp^{2-} (tpp = dianion of *meso*-tetraphenylporphyrin), the

* Corresponding authors.
E-mail address: JyhHChen@dragon.nchu.edu.tw (J.-H. Chen).

0277-5387/$ - see front matter © 2006 Elsevier Ltd. All rights reserved.
doi:10.1016/j.poly.2006.01.020

complex **1** became Ni(tpp-*N*-O) (**2**) [12]. However, until now there has been no X-ray structural data available for the diamagnetic and bridged metal [M(III)] porphyrin complexes with an oxygen atom being inserted between one metal–N unit and with a coordination number (CN) above 4 (i.e., with CN $\geqq$ 5).

In order to investigate the range of metal ions that can be inserted into H_2(tpp-*N*-O), we present the results upon replacing Ni(II) with Tl(III) in Ni(tpp-*N*-O) (**2**) forming a new complex Tl(tpp-*N*-O)(OAc) (**3**). This replacement increases the coordination number (CN) from four for **2** to six for Tl(tpp-*N*-O)(OAc) (**3**). The presence of acetate ligands in **3** plays a potential role in increasing the coordination number.

In order to figure out the structural features of oxygen and nitrogen inserted into the Tl–N bond, we also describe the synthesis and X-ray structural investigation on the metallation of 21-(4-*tert*-butyl-benzensulfonamido)-5,10,15,20-tetraphenylporphyrin [N-*p*-$HNSO_2C_6H_4{}^t$Bu-Htpp (**4**)], leading to the mononuclear complex *cis*-acetato-N-*p*-*tert*-butylbenzensulfonylimido-*meso*-tetraphenylporphyrinato-thallium(III) Tl(N-*p*-$NSO_2C_6H_4{}^t$Bu-tpp)(OAc) (**5**). Because of the large size of Tl^{3+} (r_{ion} = 1.025 Å) [13] the relative position of acetate and the 4-*tert*-butylbenzensulfonyl (^{t}BuBS) group coordinated to the Tl atom might lead to a *cis* configuration in **5** [5,8,9]. Prompted by earlier studies on the acetato exchange of Tl(tpp)(OAc) and Tl(N-NTs-tpp)-(OAc) in CD_2Cl_2(NTs = tosylimido) [8,14,15], we investigated a similar intermolecular acetato exchange for **3** and **5** in CD_2Cl_2 by ^{1}H and ^{13}C dynamic NMR methods. Thallium shows rich coupling patterns to the nuclei of the porphyrin core and to the porphyrin substituents and axial ligands. Many long-range Tl–C and Tl–H couplings to the porphyrin substituents and to the axial ligands are observed [16,17]. Moreover, there is no precedence in the literature that the magnitude of two- and three-bond thallium–carbon spin–spin coupling constants between the Tl atom and the OAc^- group of **3** and **5** depends on the electronegative substituents X (i.e., X = O in **3** and N in **5**) attached to the thallium atom. Thus, the electronegative dependence of spin–spin coupling constants $^nJ(Tl-{}^{13}C)$ (n = 2, 3) for the OAc^- ligand of **3** and **5** will be studied for the first time in the chemistry of thallium porphyrins. The compound **3** is the first thallium porphyrin complex with a Tl–O–N(Por) linkage and **5** represents the fourth thallium complex with a Tl–N(R)–N(Por) linkage reported in the literature [5,8,9].

2. Experimental

2.1. Tl(tpp-*N*-O)(OAc) (3)

A mixture of H_2(tpp-*N*-O) (0.063 g, 0.1 mmol) in CH_2Cl_2 (20 cm^3) and $Tl(OAc)_3$ (0.08 g, 0.2 mmol) in MeOH (10 cm^3) was refluxed for 3 h (Scheme 1) [12]. After concentrating, the residue was redissolved in CH_2Cl_2, dried with anhydrous Na_2SO_4, and filtered. The filtrate was concentrated and recrystallized from CH_2Cl_2–MeOH [1:2 (v/v)] yielding the blue solid of **3** (0.062 g, 7×10^{-2} mmol, 70%). Compound **3** was dissolved in toluene to crystallize out as blue crystals for single-crystal X-ray analysis. ^{1}H NMR (599.95 MHz, $CDCl_3$, 20 °C): δ 9.18 [dd, 2H, H_β

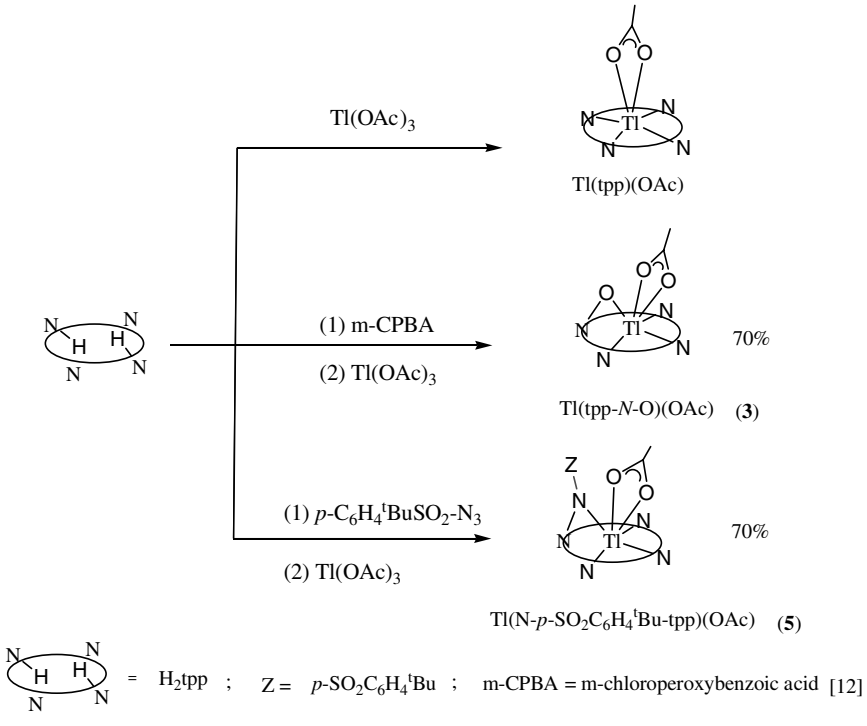

Scheme 1.

(2, 13), ^4J(Tl–H) = 13 Hz and ^3J(H–H) = 4.8 Hz], H_β (a, b) represents the 2 equiv. β-pyrrole protons attached to carbons a and b, respectively; 8.93 [dd, 2H, H_β (3, 12), ^4J(Tl–H) = 20 Hz and ^3J(H–H) = 4.8 Hz]; 8.79 [d, 2H, H_β (7, 8), ^4J(Tl–H) = 79 Hz]; 6.65 [s, 2H, H_β (17, 18)]; 8.45 [d, 2H, *o*-H (26, 28), ^3J(H–H) = 4.4 Hz], *o*-H represents *ortho* phenyl protons; 8.07 [s, 2H, *o*-H (22, 32)]; 7.72–7.81(m, 12H) for *meta* and *para* phenyl protons (*m*-, *p*-H); 0.54 (s, 3H, OAc). FAB MS, *m*/*z* (assignment, rel. intensity): 154 ($[NBA + H]^+$, 100), 614 ($[H_2tpp]^+$, 36.31), 630 ($[H_2tpp\text{-}N\text{-}O]^+$, 40.13), 631 ($[H_2tpp\text{-}N\text{-}O + H]^+$, 42.67), 833 ($[Tl(tpp\text{-}N\text{-}O)]^+$, 64.31), UV/Vis spectrum, λ/nm [$\varepsilon \times 10^{-3}$ ($M^{-1}\,cm^{-1}$)] in CH_2Cl_2: 333.2 (17.1), 477.2 (173.0), 584.4 (9.1), 626.0 (10.9).

2.2. Tl(N-*p*-$NSO_2C_6H_4{}^t$Bu-tpp)(OAc) (5)

A mixture of $Tl(OAc)_3$ (0.05 g, 1.31×10^{-4} mol) in MeOH (20 cm^3) and N-*p*-$HNSO_2C_6H_4{}^t$Bu-Htpp (0.05 g, 6.06×10^{-5} mol) in CH_2Cl_2 (50 cm^3) was refluxed for 3 h (Scheme 1) [9]. After concentrating, the residue was dissolved in CH_2Cl_2, dried with anhydrous Na_2SO_4, and filtered. The filtrate was concentrated and recrystallized from CH_2Cl_2–MeOH [1:3 (v/v)] yielding the bluish-purple solid of **5** (0.046 g, 4.23×10^{-5} mol, 70%) which was again dissolved in CH_2Cl_2 and layered with MeOH to get purple crystals for single crystal X-ray analysis. ^{1}H NMR (299.95 MHz, CD_2Cl_2, 20 °C): δ 9.05 [dd, 2H, H_β (10, 19), ^4J(Tl–H) = 17.1 Hz and ^3J(H–H) = 4.8 Hz]; 8.92 [dd, 2H, H_β (9, 20), ^4J(Tl–H) = 10.4 Hz and ^3J(H–H) = 4.8 Hz]; 8.69 [d, 2H, H_β (4, 5), ^4J(Tl–H) = 76.5 Hz]; 8.38 [d, 2H, ^3J(H–H) = 7 Hz] and 8.10 [d, 2H, ^3J(H–H) = 7 Hz] for *ortho* protons; 7.85–7.76 (m, 12H, for *meta* and *para* protons); 7.07 [d, 2H, ^{t}BuBS-$H_{3,5}$ or H (49, 51), ^3J(H–H) = 8 Hz]; 6.94 [s, 2H, H_β (14, 15)], 6.09 [d, 2H, ^{t}BuBS-$H_{2,6}$ or H (48, 52), ^3J(H–H) = 8 Hz]; 1.15 (s, 9H, *t*-butyl protons); 0.62 (s, 3H, OAc). ESI–MS, *m*/*z* (assignment, rel. intensity): 1087 ($[Tl(N\text{-}p\text{-}NSO_2C_6H_4{}^t$Bu-tpp)(OAc)$]^+$, 12.26), 1086 ($[Tl(N\text{-}p\text{-}NSO_2C_6H_4{}^t$Bu-tpp)(OAc)-H$]^+$, 16.34), 1030 ($[Tl(N\text{-}p\text{-}NSO_2C_6H_4{}^t$Bu-tpp) + 2 H$]^+$, 100), 1028 ($[Tl(N\text{-}p\text{-}NSO_2C_6H_4{}^t$Bu-tpp$)]^+$, 74.18). UV/Vis spectrum, λ/nm [$\varepsilon \times 10^{-3}$ ($M^{-1}\,cm^{-1}$)] in CH_2Cl_2: 332 (23.0), 446 (354), 555 (8.4), 609 (19.1).

2.3. Spectroscopy

Proton and ^{13}C NMR spectra were recorded at 299.95 (or 599.95) and 75.43 (or 150.87) MHz, respectively, on Varian VXR-300 (or Varian Unity Inova-600) spectrometers locked on deuterated solvent, and referenced to the solvent peak. Proton NMR is relative to CD_2Cl_2 or $CDCl_3$ at $\delta = 5.30$ or 7.24 and ^{13}C NMR to the center line of CD_2Cl_2 or $CDCl_3$ at $\delta = 53.6$ or 77.0. HMQC (heteronuclear multiple quantum coherence) was used to correlate protons and carbon through one-bond coupling and HMBC (heteronuclear multiple bond coherence) for two- and three-bond proton–carbon coupling. Nuclear Overhauser effect (NOE) difference spectroscopy was employed to determine the ^{1}H–^{1}H proximity through space over a distance of up to about 4 Å.

Positive ion mode ESI mass spectra were acquired at room temperature on a ThermoFinnigan LCQ Advantage mass spectrometer. The positive-ion fast atom bombardment mass spectrum (FAB MS) was obtained in a nitrobenzyl alcohol (NBA) matrix using a JEOL JMS-SX/SX 102A mass spectrometer. UV/Vis spectra were recorded at 20 °C on a HITACHI U-3210 spectrophotometer.

2.4. Crystallography

Table 1 presents the crystal data as well as other information for **3** and **5**. Measurements for **3** were taken on a Nonius Kappa CCD diffractometer using monochromatized Mo Kα radiation ($\lambda = 0.71073$ Å) at a temperature of 100(1) K. Measurements for **5** were taken on a Bruker AXS SMART-1000 diffractometer using monochromatized Mo Kα radiation ($\lambda = 0.71073$ Å) at a temperature of 100(2) K. Muti-scan absorption corrections were made for **3** and empirical absorption corrections were made for **5**. The structures were solved by direct methods (SHELXL-97) [18] and refined by the full-matrix least-squares method. The OAc group within **3** is disordered with an occupancy factor of 0.6 for O(2)O(3)C(45)C(46) and 0.4 for O(2′)O(3′)C(45′)C(46′). These four atoms (i.e., O(2), O(3), C(45) and C(46)) were refined with isotropic displacement parameters. All non-hydrogen atoms, except the

Table 1
Crystal data for $\mathbf{3} \cdot CH_2Cl_2$ and **5**

Empirical formula	$C_{47}H_{33}Cl_2N_4O_3Tl$ ($\mathbf{3} \cdot CH_2Cl_2$)	$C_{56}H_{44}N_5O_4STl$ (**5**)
Formula weight	977.04	1087.39
Space group	$P\bar{1}$	$P2_1/n$
Crystal system	triclinic	monoclinic
a (Å)	10.3685(4)	12.9290(8)
b (Å)	12.2132(4)	24.4703(15)
c (Å)	17.4671(6)	14.9484(9)
α (°)	71.214(2)	90
β (°)	77.251(2)	102.981(1)
γ (°)	69.573(2)	90
V (Å^3)	1947.72(12)	4608.5(5)
Z	2	4
F(000)	964	2176
D_{calcd} (g cm^{-3})	1.666	1.567
μ(Mo Kα) (mm^{-1})	4.333	3.605
S	1.088	0.959
Crystal size (mm^3)	$0.20 \times 0.08 \times 0.08$	$0.50 \times 0.41 \times 0.12$
$2\theta_{max}$ (°)	55.0	56.68
T (K)	100(1)	100(2)
Number of reflections measured	8846	11415
Number of reflections observed	7605	9395 ($I > 2\sigma(I)$)
R_1[a]	0.0426	0.0300
wR_2[b]	0.0987	0.0699

[a] $R_1 = [\sum\|F_o| - |F_c\|/\sum|F_o|]$.
[b] $wR_2 = \{\sum[w(F_o^2 - F_c^2)^2]/\sum[w(F_o^2)^2]\}^{1/2}$.

Table 2
Selected bond distances (Å) and bond angles (°) for compounds **3** · CH_2Cl_2 and **5**

3 · CH_2Cl_2			
Bond lengths			
Tl–O(2)	2.357(9)	Tl–O(3)	2.348(8)
Bond angles			
O(2)–Tl–O(3)	55.2(4)	O(1)–Tl–N(3)	83.85(14)
O(2)–Tl–N(1)	92.6(3)	O(3)–Tl–N(1)	147.7(3)
O(2)–Tl–N(2)	100.0(3)	O(3)–Tl–N(2)	98.8(3)
O(2)–Tl–N(3)	145.9(3)	O(3)–Tl–N(3)	90.8(2)
O(2)–Tl–O(1)	103.1 (2)	O(3)–Tl–O(1)	101.0(2)
N(1)–Tl–O(1)	87.51(14)	O(3)–C(45)–O(2)	121.9(9)
N(1)–Tl–N(2)	83.41(16)	Tl–O(1)–N(4)	106.2(3)
N(3)–Tl–N(2)	81.53(16)		
5			
Bond lengths			
Tl(1)–O(1)	2.337(2)	Tl(1)–O(2)	2.350(2)
Bond angles			
O(1)–Tl(1)–O(2)	55.85(7)	O(2)–Tl(1)–N(1)	93.26(8)
O(1)–Tl(1)–N(1)	148.99(8)	O(2)–Tl(1)–N(2)	94.16(9)
O(1)–Tl(1)–N(2)	100.86(9)	O(2)–Tl(1)–N(3)	145.97(8)
O(1)–Tl(1)–N(3)	91.97(8)	O(2)–Tl(1)–N(5)	111.79(9)
O(1)–Tl(1)–N(5)	102.91(8)	Tl(1)–O(1)–C(45)	91.60(18)
Tl(1)–N(5)–S(1)	133.96(14)	Tl(1)–O(2)–C(45)	91.01(18)
Tl(1)–N(5)–N(4)	109.36(17)	O(1)–C(45)–O(2)	121.5(3)
N(5)–Tl(1)–N(1)	85.08(9)	N(5)–Tl(1)–N(3)	83.80(9)

above four atoms, were refined with anisotropic thermal parameters, whereas all hydrogen atoms were placed in calculated positions and refined with a riding model. Table 2 lists selected bond distances and bond angles for complexes **3** and **5**.

3. Results and discussion

3.1. Molecular structures of 3 and 5

The X-ray molecules are depicted in Fig. 1a for the complex Tl(tpp-*N*-O)(OAc) (**3**) and in Fig. 1b for Tl(N-*p*-$NSO_2C_6H_4{}^t$Bu-tpp)(OAc)**5**. The complex **3** co-recrystallizes with 1 equiv. of CH_2Cl_2 solvent molecule in the triclinic space group $P\bar{1}$, and complex **5** recrystallizes in the monoclinic space group $P2_1/n$. In both **3** and **5**, it is obvious that the oxygen and $NSO_2C_6H_4{}^t$Bu moieties have been inserted into the Tl–N bond of acetato(*meso*-tetraphenylporphyrinato)thallium(III) Tl(tpp)(OAc) (see Scheme 1) [15].

The metal–ligand bond distances and the bond angles are summarized in Table 2. The bond distance (Å) are Tl–O(2) = 2.357(9), Tl–O(3) = 2.348(8) and Tl–O(1) = 2.126(4) and the mean Tl–N(*p*) = 2.264(4) for **3**; for **5** the values are Tl(1)–O(1) = 2.337(2) and Tl(1)–O(2) = 2.350(2) and the mean Tl(1)–N(*p*) = 2.241(2). Since the acetate of **3** was disordered, data reported involving O(2) and O(3) refer to the acetate at the higher occupancy factor of 0.6.

The geometry around Tl^{3+} is described as a distorted square-based pyramid in which the apical site is occupied

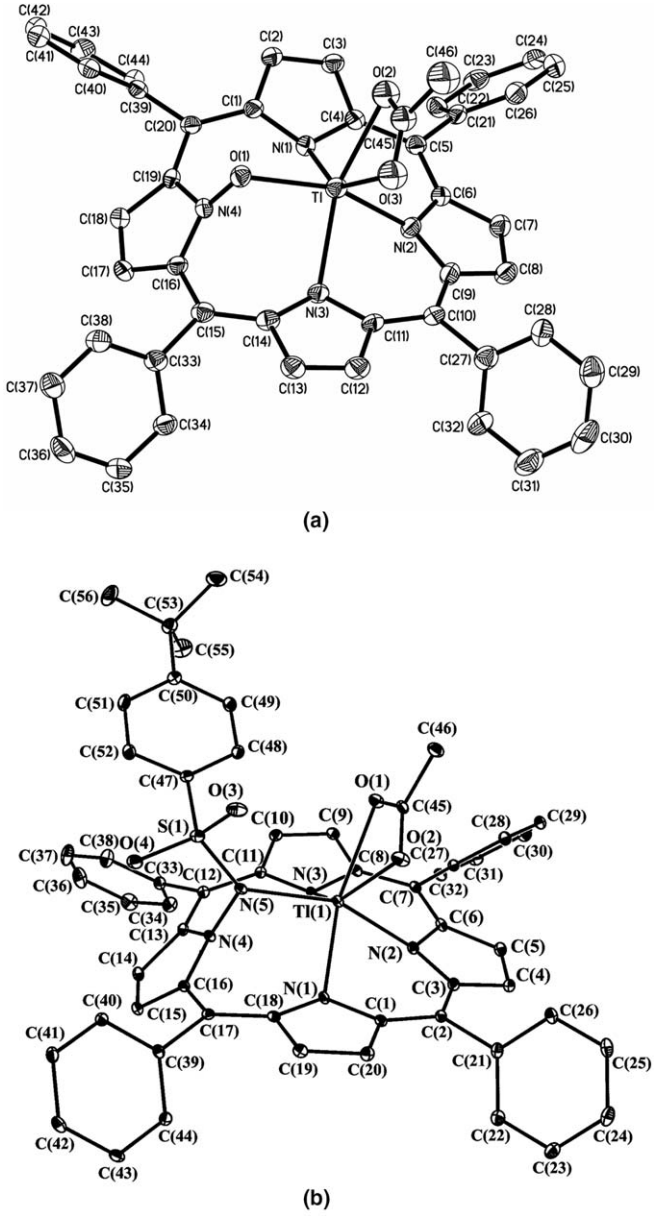

Fig. 1. Molecular configuration and atom labelling scheme for (a) Tl(tpp-*N*-O)(OAc) (**3**), (b) Tl(N-*p*-$SO_2C_6H_4{}^t$Bu-tpp)(OAc) (**5**), with ellipsoids drawn at 50% probability for **3** and at 30% probability for **5**. Hydrogen atoms for all compounds are omitted for clarity.

by a bidentate chelating OAc^- group for **3** and **5**. Fig. 2 shows the actual porphyrin skeleton of **3** and **5**. The pyrrole nitrogens N(4) (in **3** and **5**) are no longer bonded to the thallium as indicated by their longer internuclear distances, 2.831(4) Å for N(4)···Tl (in **3**) and 2.899(2) Å for N(4)···Tl(1) (in **5**). The plane of three strongly bound pyrrole nitrogen atoms (i.e., N(1)–N(3) for **3** and **5**) is adopted as a reference plane 3*N*. It is noted that the ionic radius increases from 0.63 Å for Ni^{2+} to 1.025 Å for Tl^{3+} [1,13]. Because of the larger size of Tl^{3+}, Tl and O(1) lie 1.11 and 1.34 Å, respectively, above the 3*N* plane in **3**, compared to 1.15 Å for Tl(1) and 1.30 Å for N(5) in **5** (cf. 0.05 Å for Ni(II) in Ni(OEP-*N*-O)) (Fig. 2) [1].

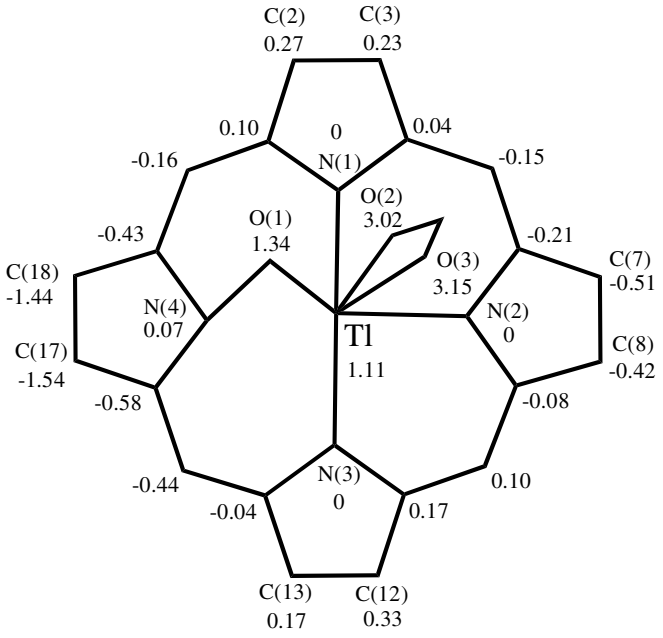

(a) Tl(tpp-*N*-O)(OAc) **3**

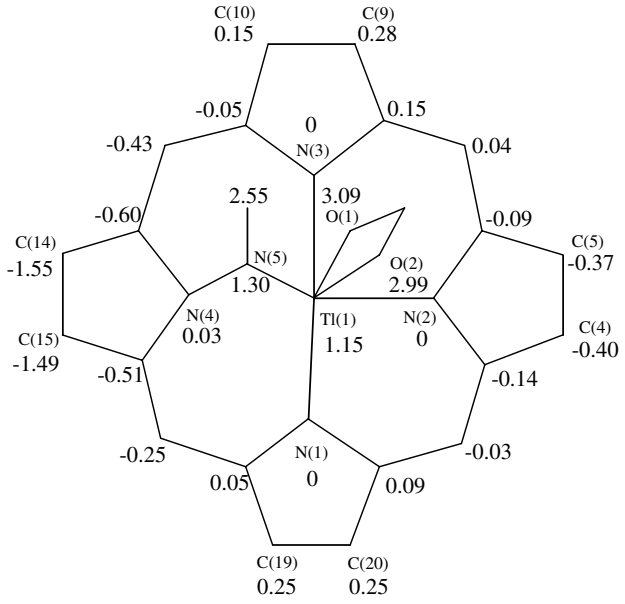

(b) Tl(N-*p*-$NSO_2C_6H_4{}^t$Bu-tpp)(OAc) **5**

Fig. 2. Diagram of the porphyrinato core ($C_{20}N_4$, M, O, ^{t}BuBS and OAc^-) of (a) **3** · CH_2Cl_2 and (b) **5**. The values represent the displacements (in angstroms) of the atoms from the mean 3*N* plane (i.e., N(1)–N(3) for **3** · CH_2Cl_2 and **5**).

The porphyrin macrocycle is indeed distorted because of the presence of the oxygen [O(1)] and the $NSO_2C_6H_4{}^t$Bu group in **3** and **5**, respectively (Fig. 2). Thus, N(4) in the **3** and **5** pyrrole rings bearing the oxygen and the $NSO_2C_6H_4{}^t$Bu group is deviated most from the 3*N* plane and oriented separately with a dihedral angle of 47.3° and of 46.7°, whereas small angles of 7.0°, 13.1° and 9.0° occur with N(1), N(2) and N(3) pyrroles for compound **3** and 6.8°, 10.8° and 7.9° with N(1), N(2) and N(3) pyrroles for compound **5**. The dihedral angles between the mean plane of the skeleton (3*N*) and the plane of the phenyl group are 49.8° [C(24)], 53.1° [C(30)], 44.7° [C(36)] and 44.0° [C(42)] for **3** and the corresponding angles are 49.4°, 57.4°, 45.0° and 53.1° for **5**.

Table 3
Comparison of distances (Å) and bond angles (°) in **3** and **5** with oxygen and nitrogen units (X) inserted between one Tl–N unit

Parameters	X = O (**3**)	Parameters	X = $NSO_2C_6H_4{}^t$Bu (**5**)
3		**5**	
O(1)–Tl	2.126(4)	Tl(1)–N(5)	2.128(2)
N(1)–Tl	2.306(4)	Tl(1)–N(1)	2.320(2)
N(2)–Tl	2.150(4)	Tl(1)–N(2)	2.153(2)
N(3)–Tl	2.335(4)	Tl(1)–N(3)	2.364(2)
N(4)···Tl	2.831(4)	Tl(1)···N(4)	2.899(2)
N(4)–O(1)	1.369(5)	N(4)–N(5)	1.386(3)
O(1)–Tl–N(2)	155.45(16)	N(5)–Tl(1)–N(2)	151.74(9)
N(1)–Tl–N(3)	121.28(15)	N(3)–Tl(1)–N(1)	118.84(8)

Table 3 contains some comparative data. The N(4)–O(1) distance of 1.369(5) Å in **3** is comparable to that in Ni(OEP-*N*-O) [1.363(6) Å] [1]. The *trans* O(1)–Tl–N(2) and N(1)–Tl–N(3) angles [155.45(16)° and 121.28(15)°] in **3** and the corresponding N(5)–Tl(1)–N(2) and N(1)–Tl(1)–N(3) angles [151.74(9)° and 118.84(8)°] in **5** indicate that both complexes are severely distorted from linearity.

In compound **3**, such a large deviation from planarity for the N(4) pyrrole is also reflected by observing a 19–22 ppm upfield shift of the C_β (C17, C18) at 112.9 ppm compared to 135.2 ppm for C_β (C2, C13), 133.7 ppm for C_β (C3, C12) and 131.8 ppm for C_β (C7, C8). In compound **5**, a similar deviation is also found for the N(4) pyrrole by observing a 16–21 ppm upfield shift of the C_β (C14, C15) at 115.7 ppm compared to 136.4 for C_β (C10, C19), 133.7 ppm for C_β (C9, C20) and 132.2 ppm for C_β (C4, C5). Similarly, the non-planarity of the porphyrins causing upfield shifts of C_β resonances were also observed with a magnitude of 16–21 ppm for Tl(N-NTs-tpp)(OAc) [8].

3.2. ^1H and ^{13}C NMR for **3** and **5** in CD_2Cl_2 and $CDCl_3$

Complexes **3** and **5** were characterized by ^{1}H (Fig. 3) and ^{13}C NMR analysis. In solution, the molecules have effective C_s symmetry with a mirror plane running through the N(2)–Tl–O(1)–N(4) unit for **3** and the N(2)–Tl(1)–N(4)–N(5) unit for **5**. There are four distinct β-pyrrole protons H_β, four β-pyrrole carbons C_β, four α-pyrrole carbons C_α, two different *meso* carbons C_{meso} and two phenyl-C_1 carbons for both the complexes.

The NMR study of **3** showed four different types of Tl–H coupling constants for H_β in CD_2Cl_2 at 20 °C (Fig. 3a). The doublet at 8.70 ppm is assigned as H_β (7, 8) with ^4J(Tl–H) = 78 Hz and the singlet at 6.64 ppm is due to H_β (17, 18). The doublet of a doublets at 9.18 ppm is due to H_β (2, 13) with ^4J(Tl–H) = 14 Hz and ^3J(H–H) = 4.2 Hz and the doublet of a doublets at 8.93 ppm is due to H_β

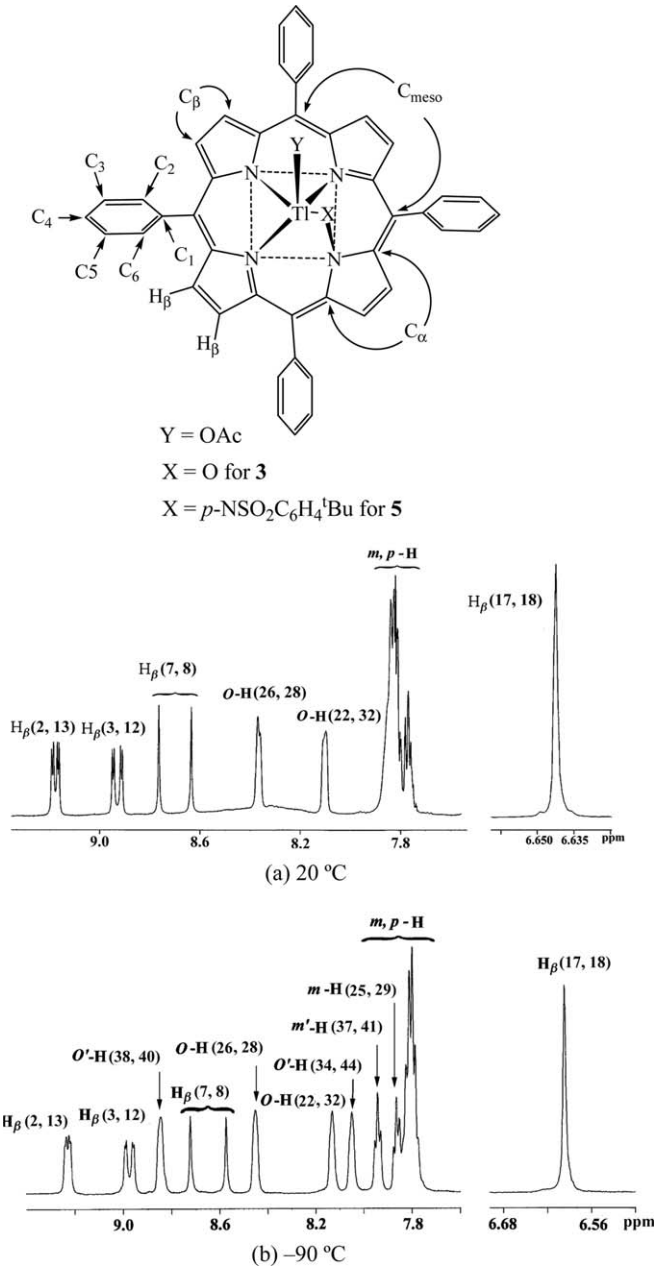

Fig. 3. ^{1}H NMR spectra for Tl(tpp-*N*-O)(OAc) at 599.95 MHz in CD_2Cl_2 showing four different β-pyrrole protons H_β and phenyl protons (*o*-H, *m*, *p*-H): (a) 20 °C; (b) −90 °C.

(3, 12) with ^4J(Tl–H) = 20 Hz and ^3J(H–H) = 4.2 Hz. Likewise, there were also four different types of Tl–^{13}C coupling constants for C_β **3** in $CDCl_3$ at 20 °C. The doublet at 131.8 ppm is due to C_β (C7, C8) with ^3J(Tl–^{13}C) = 156 Hz and the singlet at 133.7 ppm is due to C_β (C3, C12). The doublet at 135.2 ppm is due to C_β (C2, C13) with ^3J(Tl–^{13}C) = 44 Hz and the doublet at 112.9 ppm is due to C_β (C17, C18) with ^4J(Tl–^{13}C) = 80 Hz.

The NMR study of **5** showed four different types of Tl–H coupling constants for H_β in CD_2Cl_2 at 20 °C. The doublet at 8.69 ppm is assigned as H_β (4, 5) with ^4J(Tl–H) = 76.5 Hz and the singlet at 6.94 ppm is due to H_β (14, 15). The doublet of a doublets at 9.05 ppm is due to H_β (10, 19) with ^4J(Tl–H) = 17.1 Hz and ^3J(H–H) = 4.8 Hz and the doublet of a doublets at 8.92 ppm is due to H_β (9, 20) with ^4J(Tl–H) = 10.4 Hz and ^3J(H–H) = 4.8 Hz. Likewise, there were also four different types of Tl–^{13}C coupling constants for C_β **5** in CD_2Cl_2 at 20 °C. The doublet at 132.2 ppm is due to C_β (C4, C5) with ^3J(Tl–^{13}C) = 165 Hz and the doublet at 136.4 ppm is due to C_β (C10, C19) with ^3J(Tl–^{13}C) = 37 Hz. The singlet at 133.7 ppm supposedly due to C_β (C9, C20) with ^3J(Tl–^{13}C) is not observed and the doublet at 115.7 ppm is due to C_β (C14, C15) with ^4J(Tl–^{13}C) = 78 Hz. The ^{1}H NMR spectra reveal that the aromatic protons of the ^{t}BuBS group appear as a doublet at 6.94 (^{t}BuBS-$H_{3,5}$) and a doublet at 6.09 ppm (^{t}BuBS-$H_{2,6}$) for **5**. Due to the porphyrin ring current effect, all $NSO_2C_6H_4{}^t$Bu and acetato protons are shifted upfield compared to their counterparts in free $NSO_2C_6H_4{}^t$Bu and OAc^-. The above ring current effect indicates that both the $NSO_2C_6H_4{}^t$Bu and acetate ligands are bonded to Tl in **5** in the solution phase. The $NSO_2C_6H_4{}^t$Bu bonding argument is further confirmed by the result that the ^{t}BuBS–C_1 (i.e., C(47)) peak in **5** was observed at 137.6 ppm with ^3J(Tl–C) = 46 Hz. X-ray diffraction analysis unambiguously confirms that **5** is a bidentate complex in the solid phase.

Fig. 3 depicts representative ^{1}H spectra for **3** in CD_2Cl_2 at 20 and −90 °C. At 20 °C, the rotation of the phenyl group along the C_1–C_{meso} [C(5)–C(21) or C(10)–C(27)] bond is intermediately slow [19]. This intermediately slow rotation is supported by the two broad singlets at 8.36 and 8.10 ppm for the *ortho* protons *o*-H (26, 28) and *o*-H (22, 32), respectively. Moreover, the rotation of the phenyl group along the C(15)–C(33) [or C(20)–C(39)] bond is at the intermediate exchange region [21]. In this intermediate exchange region, the signals are broadened beyond detection. Hence, no signals of *o*′-H (34, 44) and *o*′-H (38, 40) have been found at 20 °C (Fig. 3a). At −90 °C, this rotation is extremely slow. Hence, the rate of intramolecular exchange of the *ortho* protons for **3** in CD_2Cl_2 is also extremely slow. The singlet at 8.85 ppm is assigned to *ortho* protons *o*′-H (38, 40) (Fig. 3b). The other singlet at 8.05 ppm is due to *ortho* protons *o*′-H (34, 44). Likewise, the singlet at 8.45 ppm is due to the *ortho* protons *o*-H (26, 28) and singlet at 8.13 ppm is due to the *ortho* protons *o*′-H (22, 32) (Fig. 3b). In a similar way, the *meta* and *para* protons appearing as multiplet (7.76–7.84 ppm) at 20 °C (Fig. 3a) changed to 7.94 [t, *m*′-H (37, 41)], 7.86 [t, *m*-H (25, 29)], 7.82 [m, *m*′-H (35, 43)], 7.81 [m, *p*′-H (36, 42)] and 7.80 [m, *m*-H (23, 31) and *p*-H (24, 30)] ppm at −90 °C (Fig. 3b). The interpretation of these data was confirmed by NOE difference spectroscopy for **3** in CD_2Cl_2 at 20 and −90 °C.

In a similar fashion, the rotation for the phenyl group of **5** in CD_2Cl_2 at 20 °C along the C(2)–C(21) [or C(7)–C(27)] bond is slow and that rotation along C(12)–C(33) [or C(17)–C(39)] is at the intermediate region. Hence, the ^{1}H resonances for the *ortho* protons of **5** were observed with two sets of doublets: one doublet at 8.38 ppm is assigned

to *ortho* protons *o*-H (26, 28) with ^3J(H–H) = 7 Hz and the other doublet at 8.10 ppm is due to *ortho* protons *o*-H (22, 32) with ^3J(H–H) = 7 Hz. Moreover, no signals of *o*′-H (38, 40) and *o*′-H (34, 44) of **5** have been detected at 20 °C.

3.3. Dynamic NMR of 3 and 5 in CD_2Cl_2

Upon cooling of a 0.02 M CD_2Cl_2 solution of **3**, the methyl proton signal of OAc^-, being a single peak at 20 °C ($\delta = 0.45$ ppm), first broadened (coalescence temperature $T_c = -89$ °C) and then split into two peaks with a separation of 12 Hz at $\delta = 0.35$ ppm at −100 °C. As the exchange of OAc^- within **3** is reversible, the results at 599.95 MHz confirm the separation as a coupling of ^4J (Tl–H) rather than a chemical shift difference. The most likely cause of loss of coupling is due to the reversible dissociation of acetate with a small dissociation constant.

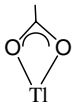

3

$$\xrightarrow[\rightleftharpoons]{CD_2Cl_2} \text{Tl(tpp-}N\text{-O)}^+ + OAc^- \qquad (1)$$

Such a scenario would lead to the change in the chemical shift with temperature and no detectable free OAc^- and Tl(tpp-*N*-O)$^+$ at low temperature, but would lead to the loss of coupling between acetate and thallium at higher temperature [20]. The chemical shift in the high-temperature limit is the average of the two species (i.e., Tl(tpp-*N*-O)(OAc) and OAc^-) in Eq. (1) weighted by their concentration. The free energy of activation $\Delta G^{\ddagger}_{184} = 39.3$ kJ/mol is therefore determined for the intermolecular exchange of OAc^- in **3**. The free energy of activation at the coalescence temperature T_c for a similar OAc^- exchange of **5** in CD_2Cl_2 is determined to be $\Delta G^{\ddagger}_{208} = 44.1$ kJ/mol. At 20 °C, intermolecular exchange of the OAc^- group for **3** is rapid as indicated by the appearance of singlet signals due to carbonyl carbons at 175.8 ppm and methyl carbons at 18.9 ppm. At −100 °C, the rate of intermolecular exchange of OAc^- for **3** in CD_2Cl_2 is slow. Hence, at this temperature, the methyl and carbonyl carbons of OAc^- are observed at δ 18.5 ppm [with ^3J(Tl–C) = 135 Hz] and 176.0 ppm [with ^2J(Tl–C) = 156 Hz] as doublets, respectively. These ^{13}C resonances are quite close to that of **5** in which the two corresponding carbons were observed in CD_2Cl_2 at δ 18.6 ppm [with ^3J(Tl–C) = 221 Hz] and 176.4 ppm [with ^2J(Tl–C) = 205 Hz] as doublets at −90 °C, but with different $^{2,3}J$(Tl–C) coupling constants. The bulky ^{t}Bu group in **5** increases the free energy of activation for the intermolecular OAc^- exchange in CD_2Cl_2 from $\Delta G^{\ddagger}_{171} = 36.0$ kJ/mol for Tl(N-NTs-tpp)(OAc) to $\Delta G^{\ddagger}_{208} = 44.1$ kJ/mol for **5** [8].

3.4. O(1) and N(5) atoms connected to α-thallium

The effect of a different electronegative atom O(1) [or N(5)] attached to the thallium(III) in **3** (or **5**) on ^2J(Tl–C) and ^3J(Tl–C) of the OAc^- ligand was studied. The importance of the thallium carbon coupling comes mainly from the Karplus-type dependence of ^3J(Tl–C) on the torsion angle $\Phi_{Tl\alpha-C\delta}(Tl_\alpha–O_\beta–C_\gamma–{}^{13}C_\delta)$ [21–23]. Hence, the complexity of the ^3J(Tl–C) coupling is primarily due to the angular dependence on Φ and also due to the substituent effects arising from the nature, position and orientation. The substituents (X) bonded to the coupled Tl_α thallium induces an additional angular dependence on the torsion angle $\Psi_{X-C\gamma}(X–Tl_\alpha–O_\beta–C_\gamma)$. Experimentally, the dependence of the ^3J(Tl–C) coupling on the torsion angles Φ, Ψ and electronegativity (χ) for **3** and **5** is shown in Table 4. Analytically, the effect upon ^nJ(Tl–C) ($n = 2, 3$) of a substituent X (X = O, N) attached to a thallium atom is defined by the difference Δ^nJ(Tl–C, X) = ^nJ(Tl–C, X)–^nJ(Tl–C, P), where ^nJ(Tl–C, X) and ^nJ(Tl–C, P) are the ^nJ(Tl–C) coupling for the X-monosubstituted Tl(tpp)(OAc) and for the parent molecule of Tl(tpp)(OAc), respectively [21]. In Table 4, the coupling constants from our study and the published ones for thallium porphyrin derivatives are provided for a comparison of the experimental Δ^nJ(Tl–C, X) values [5,8,14]. A maximum positive contribution to ^3J(Tl–C) is expected in the *transoid* arrangement ($\Phi = 180°$ and $\Psi = 180°$). The absolute values of Φ and Ψ are observed to be approximately constant around 180° and 80.1 6.8° for complexes **3**, **5** and their homologue, respectively (Table 4), therefore the magnitude of ^3J(Tl–C) in the system X–Tl_α–O_β–C_γ–$^{13}C_\delta$ shows a strong dependence on the electronegativity (χ) of the substituent X. A large negative value of Δ^3J(Tl–C, O) = −145 Hz is observed for **3** while a small negative values of Δ^3J(Tl–C, N) = −57 ± 3 Hz are assessed for **5**, **6** and **7** (Table 4) [5,8]. Likewise, the magnitude of the geminal thallium–carbon coupling constant, ^2J(Tl–C), for the OAc^- of **3** and **5** in the system X–Tl_α–O_β–$^{13}C_\gamma$ depends on the electronegativity (χ) of X (Table 4). Experimentally, a large negative value of Δ^2J(Tl–C, O) = −79 Hz is observed for **3** while a small negative value of Δ^2J(Tl–C, N) = −28 ± 3 Hz is calculated for **5**, **6** and **7** (Table 4) [5,8]. Owing to the magnitude of Δ^nJ(Tl–C, X) ($n = 2, 3$) increasing with increasing electronegativity of X, the smaller electronegativity of N(5)–$SO_2C_6H_4{}^t$Bu (with χ [N(5) = 2.98]) for **5** than the O(1) atom (with χ [O(1) = 3.44]) for **3** [24,25] results in the magnitude of $|\Delta^3J$(Tl–C, N)| = 59 Hz in **5** being smaller than that of $|\Delta^3J$(Tl–C, O)| = 145 Hz in **3** (Table 4). In a similar case, the absolute value of $|\Delta^2J$(Tl–C, N)| = 30 Hz in **5** is smaller than that of $|\Delta^2J$(Tl–C, O)| = 79 Hz in **3** (Table 4).

4. Conclusions

We have investigated two new diamagnetic and mononuclear thallium(III) porphyrin complexes **3** and **5** and their X-ray structures are established. NOE difference spectroscopies, HMQC and HMBC were employed for the unambiguous assignment of the ^{1}H and ^{13}C NMR resonances of **3** and **5** in $CDCl_3$ at 20 °C and in CD_2Cl_2 at 20 and −90 °C. In brief, the electronegativity (χ) of the X atom attached to the α-thallium nucleus correlates to the

Table 4
Effect of α-oxygen and nitrogen substituents on ^{n}J(Tl–C) ($n = 2, 3$) for the OAc^{-} group of Tl(tpp-*N*-O)(OAc), **3**, **5** and thallium porphyrin complexes in CD_2Cl_2 at low temperature[a]

Compounds	OAc		OAc		Φ (°)[c]	Ψ (°)[d]	χ (Ξ)[e]
	CH_3 ^{3}J(Tl–C)	$\Delta^{3}J$(Tl–C, X) (Hz)[b]	CO ^{2}J(Tl–C)	$\Delta^{2}J$(Tl–C, X) (Hz)[b]			
Tl(tpp)(OAc)[14] (−90 °C)	280		235				
Tl(tpp-*N*-O)(OAc) (**3**) (−100 °C)	135	−145	156	−79	−178.9	82.9	3.44
Tl(N-*p*-$NSO_2C_6H_4{}^{t}$Bu-tpp)(OAc) (**5**) (−90 °C)	221	−59	205	−30	−175.2	73.3	2.98
Tl(N-NTs-tpp)(OAc)[8] (**6**) (−110 °C)	220	−60	205	−30	178.5	−86.2	2.98
Tl(N-*p*-$NCOC_6H_4NO_2$-tpp)(OAc)[5] (**7**) (in THF-d_8, −110 °C)	227	−53	211	−24	176.6	78.1	2.89

[a] Measured in CD_2Cl_2 unless specified.
[b] $\Delta^{n}J$(Tl–C, X) = ^{n}J(Tl–C, X)–^{n}J(Tl–C, P) ($n = 2$, 3 and X = O, N), where ^{n}J(Tl–C, X) and ^{n}J(Tl–C, P) are the ^{n}J(Tl–C) coupling for the X-mono-substituted Tl(tpp)(OAc) and for the parent molecule of Tl(tpp)(OAc).
[c] The torsion angle $\Phi(Tl_\alpha–O_\beta–C_\gamma–{}^{13}C_\delta)$ is the dihedral angle between coupled atoms Tl_α and C_δ.
[d] The torsion angle $\psi(X–Tl_\alpha–O_\beta–{}^{13}C_\gamma)$ is the dihedral angle between C_γ and electronegative X.
[e] Pauling scale value calculated by electronegativity equalisation, where Ξ = O for **3**, N–^{t}BuBs for **5**, N–NTs for **6** and $NCOC_6H_4NO_2$ for **7** [24].

magnitude of the $\Delta^{2,3}J$ (Tl–C, X) coupling for the Tl(O_2CCH_3) fragment in the thallium porphyrin system. The two compounds, despite the different electronic and steric properties for O(1) in **3**, and for the *N*-imido-benzensulfonyl group in **5**, the structural deformations occurring in the tetrapyrrole macrocycles are similar.

Acknowledgement

The financial support from the National Science Council of the ROC under Grant NSC 93-2113-M-005-015 is gratefully acknowledged.

Appendix A. Supplementary data

Fig. S1 shows the ^{1}H NMR spectrum of **5** in CD_2Cl_2 at 20 °C. Figs. S2 and S3 show the HMQC and HMBC spectra of **3** in CD_2Cl_2 at 20 °C. CCDC 288278 (for **3**) and CCDC 261305 (for **5**) contain the supplementary crystallographic data for this paper. Copies of this information may be obtained free of charge from The Director, CCDC, 12 Union Road, Cambridge, CB2 1EZ, UK on request (fax: +44 1223 336 033; e-mail deposit@ccdc.cam.ac.uk or www: http://www.ccdc.cam.ac.uk). Supplementary data associated with this article can be found, in the online version, at doi:10.1016/j.poly.2006.01.020.

References

[1] A.L. Balch, Y.W. Chan, M.M. Olmstead, J. Am. Chem. Soc. 107 (1985) 6510.
[2] Y.I. Li, C.S. Chang, J.Y. Tung, C.H. Tsai, J.H. Chen, F.L. Liao, S.L. Wang, Polyhedron 19 (2000) 413.
[3] C.H. Chen, Y.Y. Lee, B.C. Liau, S. Elango, J.H. Chen, H.Y. Hsieh, F.L. Liao, S.L. Wang, L.P. Hwang, J. Chem. Soc., Dalton Trans. (2002) 3001.
[4] F.A. Yang, J.H. Chen, H.Y. Hsieh, S. Elango, L.P. Hwang, Inorg. Chem. 42 (2003) 4603.
[5] C.S. Chang, C.H. Chen, Y.I. Li, B.C. Liau, B.T. Ko, S. Elango, J.H. Chen, L.P. Hwang, Inorg. Chem. 40 (2001) 2905.
[6] H.J. Callot, B. Chevrier, R. Weiss, J. Am. Chem. Soc. 100 (1978) 4733.
[7] J.P. Mahy, P. Battioni, D. Mansuy, J. Am. Chem. Soc. 108 (1986) 1079.
[8] J.Y. Tung, J.I. Jang, C.C. Lin, J.H. Chen, L.P. Hwang, Inorg. Chem. 39 (2000) 1106.
[9] W.Z. Shil, K.Y. Cho, C.W. Cheng, J.H. Chen, S.S. Wang, F.L. Liao, J.Y. Tung, H.Y. Hsieh, S. Elango, Polyhedron (2006) in press.
[10] M.M. Olmstead, R.J. Cheng, A.L. Balch, Inorg. Chem. 21 (1982) 4143.
[11] A.L. Balch, Y.W. Chan, M.M. Olmstead, M.W. Renner, J. Am. Chem. Soc. 107 (1985) 2393.
[12] (a) H. Tsurumaki, Y. Watanabe, I. Morishima, Inorg. Chem. 33 (1994) 4186;
(b) L.E. Andrews, R. Bonnett, R.J. Ridge, E.H. Appelman, J. Chem. Soc., Perkin Trans. 1 (1983) 103.
[13] J.E. Huheey, E.A. Keiter, R.L. Keiter, Inorganic Chemistry, 4th ed., Harper Collins College Publishers, New York, 1993, pp. 117, 292.
[14] J.C. Chen, H.S. Jang, J.H. Chen, L.P. Hwang, Polyhedron 10 (1991) 2069.
[15] S.C. Suen, W.B. Lee, F.E. Hong, T.T. Jong, J.H. Chen, L.P. Hwang, Polyhedron 11 (1992) 3025.
[16] K.M. Kadish, K.M. Smith, R. Guilard, The Porphyrin Handbook, vol. 5, Academic Press, London, 2000, pp. 45–46.
[17] A.G. Coutsolelos, D. Daphnomili, Inorg. Chem. 36 (1997) 4614.
[18] G.M. Sheldrick, SHELXL-97, Program for the Refinement of Crystal Structure from Diffraction Data, University of Gottingen, Germany, 1997.
[19] R.S. Drago, Physical Methods for Chemists, 2nd ed., Saunder College Publishing, New York, 1992, pp. 290–295.
[20] J.P. Jenson, E.L. Muetterties, in: L.M. Jackman, F.A. Cotton (Eds.), Dynamic Nuclear Magnetic Resonance Spectroscopy, Academic press, New York, 1975, pp. 299–304.
[21] J.S. Fabian, J. Guilleme, E. Diez, J. Mol. Struct. (Theochem.) 426 (1998) 117.
[22] M. Morvai, T. Nagy, A. Kocsis, L.F. Szabo, B. Podanyi, Magn. Reson. Chem. 98 (2000) 343.
[23] R.H. Contreras, J.E. Peralta, Prog. Nucl. Magn. Reson. 37 (2000) 321.
[24] H. Liu, Q. Wang, L. Liu, J. Chem. Educ. 69 (1992) 783.
[25] S.G. Bratsch, J. Chem. Educ. 62 (1985) 101.